Mapping Geothermal Permeability Using Passive Seismic Emission Tomography Constrained by Cooperative Inversion of Active Seismic and Electromagnetic Data

Ian Warren

U.S. Geothermal Inc., 390 E. Parkcenter Blvd., Suite 250, Boise, ID 83706

iwarren@usgeothermal.com

Erika Gasperikova

Lawrence Berkeley National Laboratory, One Cyclotron Road, M/S: 74R316C, Berkeley, CA 94720

egasperikova@lbl.gov

Satish Pullammanappallil

SubTerraSeis, 2317 Red Maple Ct., Reno, NV 89523

satishpullam@gmail.com

Michael Grealy

Microseismic Inc., 1391 N Speer Blvd, Ste. 330

Denver, CO 80204

mgrealy@microseismic.com

Keywords: geothermal, passive seismic, electromagnetic

ABSTRACT

Preliminary results from a DOE-funded Subsurface Technology and Engineering R&D (SubTER) project to advance imaging and characterization of geothermal permeability are encouraging. Newly acquired electromagnetic data were used to develop 3-D resistivity volumes and dense, passive seismic arrays were used to create energy volumes with passive seismic emission tomography (PSET). These new datasets are being combined with historic drilling, active seismic, and potential fields data to generate 3-D permeability maps. Additionally, cooperative inversion of active seismic data and electromagnetic data is aimed at optimizing their utility for generating robust velocity models and potentially enhancing imaging of geothermal pathways and fluids.

Final passive seismic and electromagnetic data collections were completed at two U.S. Geothermal Inc. projects in October 2017. At San Emidio, NV the study area partly overlaps a geothermal resource that currently produces 9 net megawatts per hour. Drilling to the south of the currently exploited geothermal resource and within the SubTER study area has discovered a hotter resource than previously identified anywhere within the San Emidio Valley. Permeability associated with the new resource coincides with energy anomalies defined by PSET and with low resistivity anomalies defined by electromagnetic data while the structural setting of these anomalies is constrained by drilling, gravity, and magnetics.

At Crescent Valley a mineralized range-front fault system hosts hot springs that discharge near-boiling fluid with chalcedony geothermometer temperature of 314F. Energy anomalies defined by PSET and low resistivity anomalies defined by electromagnetic data occur down-dip from and basinward of the hot springs. These anomalies are located where range-front-parallel faulting potentially intersects faulting associated with a NNW-trending horst that is defined by drilling and geophysics. In addition to the range-front-fault-hosted hot springs, geothermal fluid also is associated with the horst underlying the valley floor based on blow outs of historic mineral exploration core holes.

Preliminary assessment of integrated datasets suggests that a robust 3-D permeability map can be created using electromagnetic and dense passive seismic datasets when they are combined with drilling and potential fields datasets that help constrain the structural and geological controls on geothermal permeability. Cooperative inversion of seismic and electromagnetic datasets can refine generation of velocity models to optimize processing and interpretation of passive seismic data. The project aims to define a methodology that will provide a general toolset applicable to geothermal exploration and exploitation.

1. INTRODUCTION

Geophysical methods have been applied to exploration and development of geothermal resources for decades, and geophysical techniques have continued to advance in terms of resolution and robustness of inversion constraints, particularly owing to ever greater

computational capabilities. Despite the ongoing advancements, geophysical techniques still fail to consistently image permeability, and no technique has been developed to effectively and robustly map subsurface permeability of geothermal resources. The targeting of permeability is perhaps the greatest risk to geothermal drilling success, so the lack of a robust tool to map permeability is not a trivial problem.

Ongoing efforts to address the problem of mapping subsurface geothermal permeability rely on integration of multiple geologic, geochemical, and geophysical datasets with more advanced efforts adding novel geophysical inversion techniques and computationally intense data processing. The integration methodologies are largely driven by enhancement of geological models with geophysical datasets and interpretations of geologic controls on permeability. Geochemistry provides additional information about the complexity of the permeability, and commonly is derived from water samples that are sampled from that permeability. More advanced geophysical methodologies attempt to identify unique signals associated with known permeable zones in the subsurface. The attempts to identify unique signals associated with known subsurface permeability have yet to successfully map such a signal throughout a geophysical inversion volume thereby creating a 3-D map of permeability (e.g., Casteel et al., 2016). It is noteworthy that one of the oldest geothermal exploration methods, temperature gradient drilling, is perhaps still the best method to map permeability via temperature as proxy.

The magnetotelluric (MT) method has been developed into a useful technique for imaging geothermal reservoirs, especially when combined with other datasets, e.g., seismic or gravity. MT uses naturally occurring broadband electromagnetic (EM) fields over the Earth's surface that arise from regional and worldwide thunderstorm activity and from interaction of the solar wind with the Earth's magnetosphere. The amplitude, phase, and directional relationship between electric (E) and magnetic (H) fields on the surface depend on the subsurface distribution of electrical resistivity, which is largely driven by the properties and distribution of fluids. The measured MT impedance is defined as the ratio of electric and magnetic fields. Measured responses change with frequency such that high frequencies are sensitive to shallow depths and lower frequencies penetrate to greater depths, and these data are used to invert for subsurface electrical properties (Vozoff, 1991).

The oil and gas industry, especially since the massive expansion of shale resources exploitation, has used passive seismic techniques, including seismic emission tomography (SET), to understand permeability fairways and to monitor frack jobs, i.e., creation of new permeability (Geiser et al., 2012; Lacazette and Morris, 2015; Sicking et al., 2012). Though some geothermal fields are monitored with passive seismic arrays in order to monitor and map microearthquake (MEQ) hypocenters, we are not aware of SET techniques, as used by the oil and gas industry to map permeability, having been applied to the problem of geothermal permeability. Our DOE-funded (DE-FOA-0001445; Federal: $1,497,017, US Geothermal: $449,378) experiment proposes to advance the effective imaging of geothermal permeability by testing SET techniques used by the oil and gas industry to map fracture-controlled permeability. Additionally, refinement of cooperative inversion of seismic and EM data will enhance the recognized capabilities of both those techniques, imaging of discrete structures and imaging of conductive geothermal brine, respectively, to provide a more robust methodology for deploying these technologies toward the problem of mapping geothermal permeability.

2. PROJECT LOCATIONS, GEOLOGY, AND GEOPHYSICS

New passive seismic and magnetotelluric data collections have been completed at San Emidio and Crescent Valley, Nevada (Figure 1). At San Emidio, geothermal power has been produced since 1987. U.S. Geothermal purchased the Empire power plant in 2008 and output increased to 9 net megawatts after a new power plant was installed in 2012. Abundant production, drilling, geologic, and geophysical data mean that the subsurface is well constrained. Additionally, recent drilling at San Emidio has identified new, higher temperature resource south of the currently producing field. In contrast, much less is known about the subsurface at Crescent Valley where project activities are focused in the area of hot spring discharges along the Crescent Valley fault with geothermometry indicating a ~150C reservoir at depth. The two locations allow testing of permeability mapping techniques at a well constrained "training" site and also at a "greenfields" exploration site. At both sites data collection occurs in the vicinity of step-overs in range front faults; sites favorable for development of geothermal systems (Faulds et al. 2011). Additionally, Crescent Valley was deemed one of the most prospective areas for discovering a geothermal system based on results of University of Nevada Reno's Play Fairway analysis project (Faulds et al. 2016).

Figure 1: Project Locations. San Emidio power plant and vicinity, Washoe Co., NV and Crescent Valley, Eureka Co., NV.

2.1 San Emidio Geologic and Geothermal Setting

The San Emidio Desert is located within the actively extending northwestern Basin and Range of Nevada, approximately 100 km north of Reno. San Emidio lies within a transtensional tectonic setting between northwest-directed shear to the west associated with the Walker Lane and west-northwest to east-west extension to the east associated with the western Basin and Range (Bennett et al., 2003; Hammond and Thatcher, 2005; Hammond et al. 2009).

The geology of the eastern San Emidio Desert is known from exposures in the northern Lake Range and from drilling associated with geothermal exploration and development in the basin to the west that lies in the hanging wall of the Lake Range fault (Figure 2). Triassic-Jurassic metasedimentary and metavolcanic rocks of the Nightingale Sequence (Bonham and Papke, 1969) are overlain by Tertiary volcanic and sedimentary rocks belonging to the Middle Miocene Pyramid Sequence (Drakos, 2007). In the southeastern part of the San Emidio Desert where geothermal exploration and development are primarily focused, the Pyramid Sequence is dominated by intermediate to mafic composition lavas with intercalated tuff and tuffaceous sediments, and is overlain by Tertiary-Quaternary volcaniclastic sedimentary rocks and minor tuff. Exposures to the north of and in the subsurface of the geothermal resource area are variably hydrothermally altered with weak to intense and spotty to pervasive clay and silica alteration (Figure 2). Precious metals mineralization at the Wind Mountain Mine to the north of the San Emidio geothermal field is associated with pervasive silicification and epithermal veins hosted in Miocene to Pliocene (?) sedimentary rocks (Wood, 1990). Quaternary deposits include Pleistocene Lake Lahontan silt, sands, and tufa with variable hydrothermal alteration localized along the San Emdio fault (Rhodes et al. 2010).
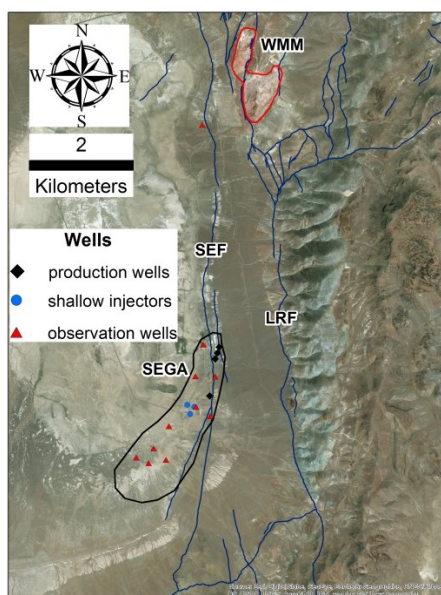
Figure 2: Southeastern San Emidio Desert and the San Emidio Geothermal Area (SEGA), Washoe County, NV. LRF-Lake Range fault; SEF-San Emidio fault; WMM-Wind Mountain Mine. Active and monitor wells show the extent of the currently defined resource area which is open to the south and west. Bleached and Fe-stained rocks along the SEF and LRF and in the vicinity of the WMM are hydrothermally altered. Green-blue-gray exposures in the footwall of the west-dipping LRF are Mesozoic metamorphic rocks which are overlain by Tertiary rocks that dip to the east. Dark blue faults are from Rhodes et al. (2011).

The San Emidio Geothermal Area has been known since anomalous temperature gradient wells were drilled in the 1970s. A shallow (100-300' below surface) resource was put into production in 1987 with a 3.6 MW binary plant; hot water also was used to support dehydration facilities in the 1990s through the early 2000s. Initial, shallow production wells were converted to injection wells after deeper production wells were drilled to the north along the San Emidio fault (Figure 2) following cooling of the shallow reservoir. U.S. Geothermal Inc. acquired the geothermal plant and leases in 2008, and a new 14.7 MW plant was commissioned in 2012. Over the life of the project, production has ranged from <3000 gpm to >4500 gpm at temperatures of 140-148C. From 2015 to 2017, drilling south of the producing field discovered a new, hotter (>160C) resource that is currently in the early development stages.

San Emidio wells produce primarily from depths of ~1700 to 2300' below surface from fractures hosted by silicified tuff and intermediate to mafic composition lavas. The top of the reservoir generally follows the contact between overlying, mechanically weak, commonly clay-altered volcaniclastic rocks and underlying, mechanically strong, silicified tuff and lavas. The shallow injection zone is associated with massive silicification of tuff and tuffaceous sedimentary rocks; it is poorly connected to production wells, and most injectate flows north in the shallow subsurface. The newly discovered resource to the south has a similar geologic setting with the reservoir hosted by fractured, silicified tuff and lava and overlain by clay-altered, volcaniclastic rocks. Based on limited flow test data, it is poorly connected to the currently producing reservoir.

2.2 San Emidio Geophysics

Though several geophysical campaigns were carried out prior to U.S. Geothermal Inc.'s acquisition in 2008, this brief summary focuses on surveys completed during U.S. Geothermal Inc.'s ownership. Initial work by U.S. Geothermal Inc. focused on ground gravity and magnetics, and these surveys were extended to the south and west in 2016. Most notable from these datasets are features within the step-over in the range front fault south of the San Emidio wellfield. A refined structural model of the current study area has been guided by 2-D modeling of gravity data (Figure 3).
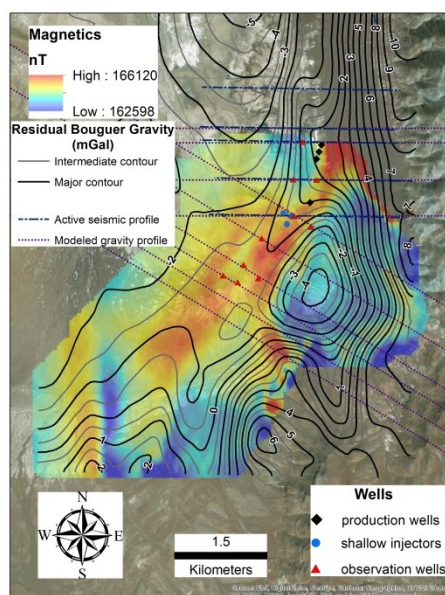
Figure 3: San Emidio ground gravity and magnetics. Magnetics symbolized with warm to cool colors (high to low nanotesla values) are overlain by residual Bouguer gravity contours to show the complex structural setting of the range-front step-over. Also shown are locations of modeled gravity profiles and historic 2-D seismic lines.

From 2010 to 2014 DOE-funded innovative exploration research completed 9 active seismic profiles (5 southern most shown in Figure 3), detailed structural and slip tendency analyses, PSInSAR ground deformation studies (Eneva et al., 2011), and drilling and deepening of 8 observation wells to test these methods (Teplow and Warren, 2015). The active seismic profiles imaged the main range-front fault, but resolution of other structures, particularly in volcanic +/-hydrothermally altered rocks, was generally poor. Velocity modeling of the seismic profiles showed complex patterns of velocity gradient related to structure and possibly hydrothermal alteration (Figure 4). Slip tendency analyses confirmed north- to north-northeast-trending faults as most likely to dilate in the current regional stress regime. PSInSAR highlighted probable structural boundaries to subsiding areas associated with production wells, and inflating areas associated with shallow injection. Drilling intersected highest temperatures drilled in the field (162C) adjacent to and below the main production zone, and expanded the known permeable reservoir to the south (Figures 2 and 3; southernmost production well).
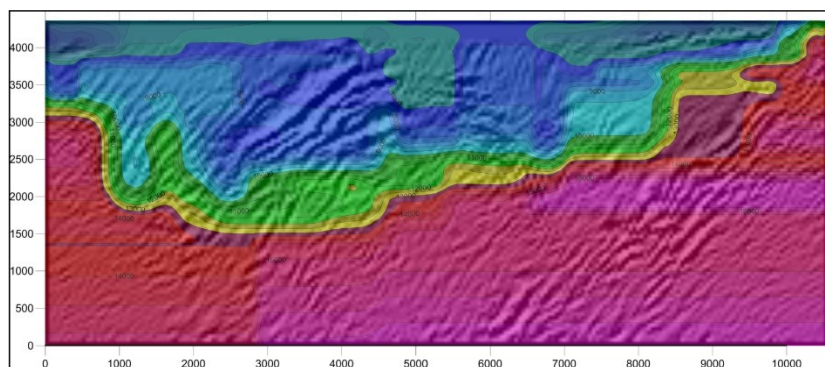
Figure 4: San Emidio Seismic Line 9 (southernmost, Figure 3). P-wave velocity model overlain on migrated seismic reflection profile shows structural complexity across the geothermal reservoir.

2.3 Crescent Valley Geologic and Geothermal Setting

The Crescent Valley geothermal project area is located in Eureka County, NV. It is bounded to the east by the Cortez Range and to the northwest by the Dry Hills. U.S. Geothermal Inc. acquired the property in 2014 and has expanded the property to include ~30,000 acres of private and Federal geothermal leases (Figure 5). Surface geothermal manifestations occur at the southeast end of the property along the Crescent Valley fault and at the northwest end of the property along the Dry Hills fault. The middle of the property was previously drilled by mineral explorers who lost control of core holes when they intersected artesian, flashing fluid at depths of ~2000' below surface. Geothermometry of hot spring discharges suggests reservoir temperatures at depth in excess of ~150C.
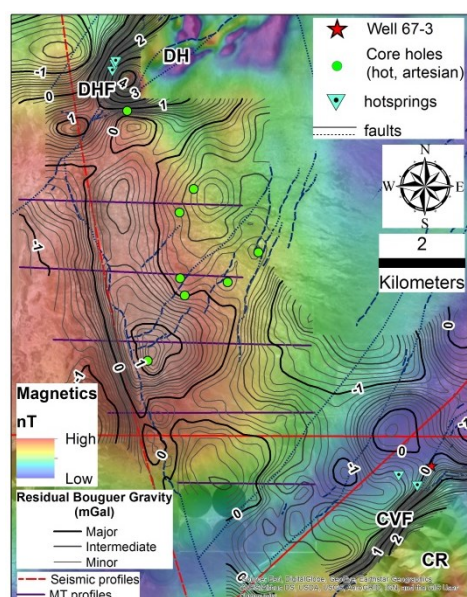
Figure 5: Crescent Valley geothermal project, Eureka Co., NV. CR-Cortez Range; CVF-Crescent Valley fault; DH-Dry Hills; DHF-Dry Hills fault. This study is focused in the area where hot springs discharge from the CVF. Mapped faults are from McConville et al (2017). Residual Bouguer gravity contours are overlain on total magnetic intensity.

Most of the Crescent Valley property is covered with Tertiary-Quaternary sedimentary rocks. At the northwest end of the property, the southern end of the Dry Hills, known as Hot Springs Point, Tertiary volcanic rocks, Jurassic granodiorite, and Paleozoic metasedimentary rocks make up the footwall of a northwest-dipping range-front fault (DHF) along which discharge chloride-bicarbonate springs. At the southeast end of the property, Jurassic granodiorite makes up the footwall of the northwest-dipping Crescent Valley fault (CVF). Fluids discharged from hot springs along the CVF are distinct from those at Hot Springs Point with notably less bicarbonate, and they are near-boiling with silica geothermometry indicating reservoir temperatures >150C. Mineral exploration core holes, gravity, and 1980s active seismic profiles identify an uplifted horst that stretches across the valley, trending north-northwest from the Crescent Valley fault south of the aforementioned hot springs to Hot Springs Point. The horst is made up of Paleozoic carbonate and siliciclastic rocks intruded by Jurassic granodiorite, and overlain by Tertiary mafic lava and Tertiary-Quaternary sedimentary rocks. At Hot Springs Point and in the vicinity of hot springs along the CVF, epithermal precious metals mineralization and associated hydrothermal alteration are present and have been explored by multiple companies.

The Crescent Valley property and vicinity was explored in the late 1970s by Chevron who completed 31 shallow temperature gradient wells. Anomalous gradients were identified outward from Hot Springs Point up to ~3 km and outward from CVF hot springs >6 km, defining large areas of anomalous heat flow. Core holes in the middle of the valley and adjacent to the horst were drilled in the 2000s by Montezuma Mines (Figure 5). Some of these encountered artesian, flashing fluid, but no fluid samples were collected and no equilibrated downhole temperatures were measured. In late 2015 and early 2016, U.S. Geothermal drilled well 67-3. A relatively shallow intersection of the range-front fault showed modest permeability and temperature; temperature surveys suggest downhole flow of cool water and chemistry indicates dilution relative to hot spring samples. Well 67-3 drilled through silicified, brecciated, and mineralized rocks, multiple splays of the range-front fault system, and variably silicified granodiorite down to a depth of ~1590' before intersecting fresh to weakly altered, footwall granodiorite.

2.4 Crescent Valley Geophysics

A number of geophysical surveys have been completed at Crescent Valley related to hydrocarbon and minerals exploration. These include four active seismic profiles, ground gravity, gravity gradiometry, ground magnetics, aeromagnetics, and 2-D electromagnetic profiles (Figure 5). U.S. Geothermal Inc. added dense ground gravity in the vicinity of hot springs along the CVF in 2015. Since then additional work has been done in the area including additional gravity data collection, seismic reinterpretation, structural mapping, and fluid sampling associated with the University of Nevada Reno's DOE-funded, Play Fairway project (McConville et al. 2017).

The current study is focused in the vicinity of the hot springs discharging along the CVF. Preliminary structural modeling has been guided by surface measurements along the trace of the CVF, orientation of veins, breccia, and hydrothermal alteration along and adjacent to the CVF, 2-D modeling of gravity, and interpretation of the east-west oriented, historic 2-D seismic profile.

3. SUBTER PROJECT DATA COLLECTIONS

Passive seismic data collections were completed at San Emidio and Crescent Valley in late 2016 by Microseismic Inc. At San Emidio, 1302 stations with 6 wired geophones connected to OYO GXR recorders together collected data for nearly 180 hours. At Crescent Valley the same equipment deployed at 989 stations together collected data for 75 hours. Surveys were designed to focus on an area of the subsurface approximately 1700m x 2200m x 300m and initial processing focused on depths of ~600m to 900m below surface. Preliminary processing used a simple velocity model that was guided by the velocity structure of seismic line 9 at San Emidio and

modified to create best matches to downhole string shots in wells near the center of the passive seismic arrays. Several large discrete events were also used to calibrate the San Emidio velocity model. Residual static solutions applied across the entire datasets were applied to bring all the traces used in the beamformer into phase. The average absolute positional error of the string shots used to verify this calibration is 1m in the X and Y directions and 3m in the Z direction. For San Emidio a list of discrete microseismic events and a PSET volume of acoustic energy transformed into Z-scores were delivered. For Crescent Valley no discrete events were identified, so only a PSET volume of acoustic energy transformed into Z-scores was delivered.

MT data collection at San Emidio started in late 2016; due to low natural signals the results were not satisfactory, and measurements over a portion of the survey area were repeated and completed in summer 2017. Data collection at Crescent Valley was completed in September 2017. The MT data acquisition (250 Hz-0.001 Hz) at both locations was done by Quantec Geoscience USA Inc (Figure 6). In addition to these two surveys, at Crescent Valley, Quantec also acquired Audio-MT (AMT) (10 kHz – 0.001 Hz) data along 10 profiles, and provided 2-D inversions and interpretation of these data. The interpretation of AMT data was aimed at identifying faults and shallow structures in the study area.
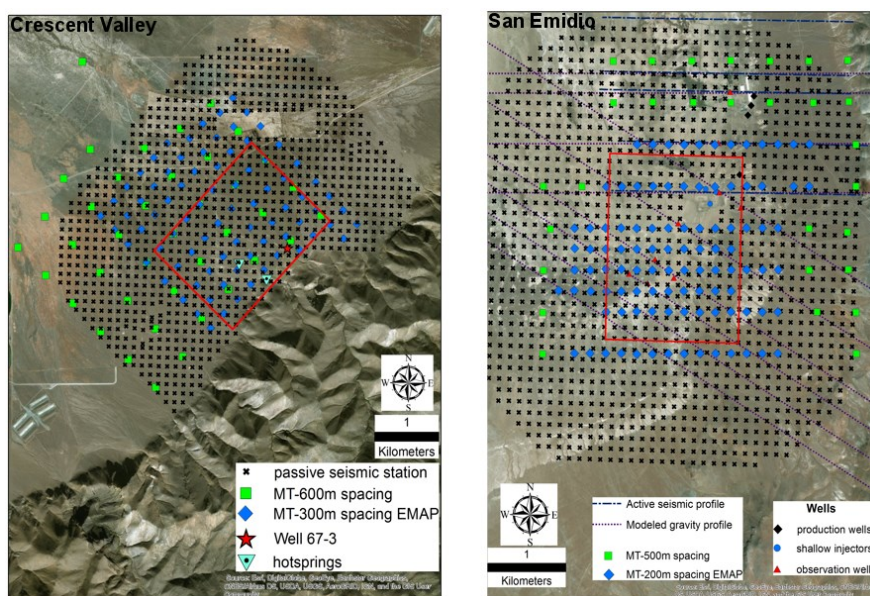
Figure 6: Passive seismic and electromagnetic data collections at Crescent Valley (left) and San Emidio (right). Red boxes show the ~1700m x 2200m x 300m focus area.

3.1 Passive Seismic Processing

The passive seismic data collected at the San Emidio site were processed using two closely related passive seismic imaging techniques based on beamforming of the high-frequency approximation of the wave equation. The first technique applied to the data is aimed at identifying discrete events with an impulsive character (Duncan and Eisner, 2010) using the Microseismic Inc. (MSI) Passive Seismic Emission Tomography algorithm using a time window for imaging of 50 milliseconds. In order to estimate the hypocenter location and origin time of a microseismic event, the array is beamformed onto a series of points in the subsurface. Beamforming is accomplished using travel-time correction and stack response. The stack is performed across all recorded traces for the entire length of the recording interval and for each cell in the processing volume, and each beamformed trace is an estimate of the acoustic history of the focus point. Once the family of related responses for an event is isolated, a maximum likelihood estimator is used to finalize the event location and origin time. The direction of first motion and the observed amplitude across the array were used to derive focal mechanisms for several large, discrete events at San Emidio, while no discrete events other than the downhole string shot were identified at Crescent Valley.

The second technique, Ambient Passive Seismic Imaging, is a close analog to the more conventional approach described above and accomplished using MSI's repetitive Passive Seismic Emission Tomography using a time window for imaging of 1 hour. The principal difference is that it relies on longer duration stacking within the beamformer to suppress random noise and allow for smaller ambient or repetitive signals to image. The increased duration of the stacking window sacrifices precise source time for increased noise suppression; therefore, it is not possible to estimate a discrete hypocenter or event origin time from a formed beam. The technique provides a holistic view of acoustic history using the long duration aggregation of multiple formed beams (Jeremic at al., 2016). Figure 7 schematically illustrates the difference between the processing methods. Throughout the text, we use PSET to refer to MSI's repetitive passive seismic emission tomography, in contrast to discrete events identification with the passive emission tomography algorithm.
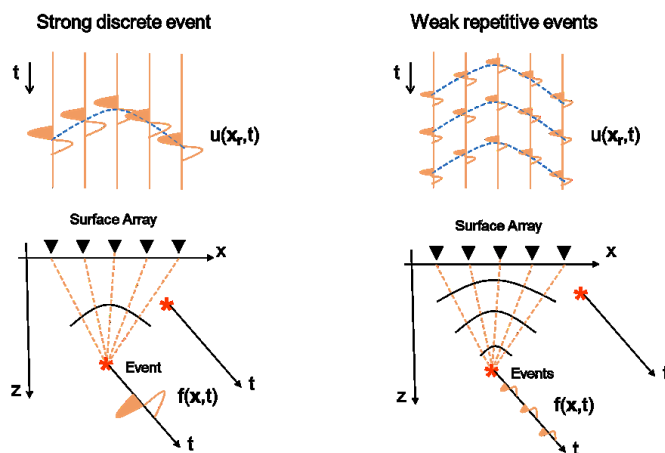
Figure 7. Schematic illustration of the variation between Microseismic Inc.'s processing techniques.

3.2 Magnetotelluric data processing and inversion

MT data were processed using the traditional remote reference approach with remote sites located 30-60 miles away from the survey area. The data were also processed using multi-station robust processing (Egbert, 1997) with at least four stations acquired simultaneously.

MT data at San Emidio were collected with the configurations shown in Figure 8. Each standalone sounding site was configured with L-shaped magnetic sensors and 200 m long E-field dipoles (Ex, Ey) (Figure 8, left); sites along profile lines used double (mirrored) L configurations (Figure 8, right). This configuration, with continuous sampling of the E-field along the profile, is called an electromagnetic array profiling (EMAP). The survey area was ~5x5 km, and 2D MT inversion was done along 10 profiles running east-west. The resistivity structures recovered by 2D inversion were then stitched into a 3D resistivity cube by interpolating between the profile lines.
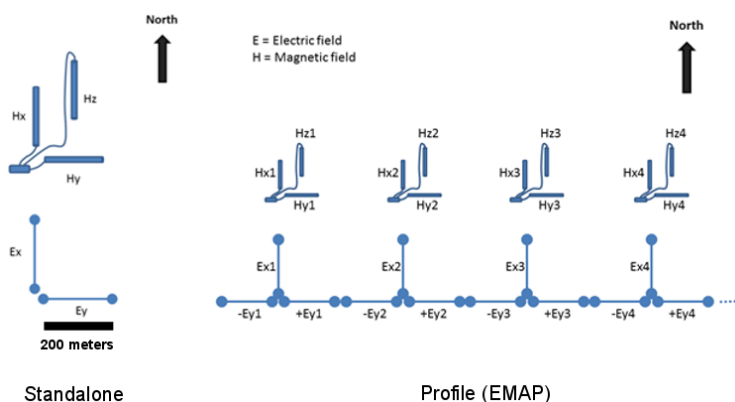
Figure 8: MT sounding site configurations

MT data at Crescent Valley were collected with the standalone sounding site configuration (Figure 8) over a survey area of ~6x4 km. 2D MT inversions were done along profiles running perpendicular to the range-front fault (CVF). The results were then stitched into a 3D resistivity cube by interpolating between the profile lines.

4. PROPOSED SEISMIC-MT COOPERATIVE INVERSION STRATEGY

At present, work related to cooperative inversion is only getting started. Cooperative inversion will aim to optimize locating subsurface permeability by combining the ability of seismic velocity structure to identify discrete structures and the ability of MT data to map subsurface regions saturated with conductive geothermal brine. Additionally, density models derived from gravity data will be used to constrain and revise structural interpretations. Our approach will also attempt to incorporate prestack depth images to further constrain the models. The objective of this approach is to improve and refine existing velocity and resistivity models while at the same time determining relationships between these attributes and subsurface permeability.

The proposed approach entails preprocessing, analysis, and optimization steps. During preprocessing, consistent models will be derived for each data type using the geographic intersection of each data type. Secondary models, e.g., gradients, will be generated as required. Data analysis will explore the relationships between data types and the structural patterns common to all data types. Pattern recognition techniques, e.g., clustering and self-organizing maps, will be used to evaluate and validate relationships and patterns. Using the analytical results, an optimal solution for velocity and resistivity model improvement will be explored using machine learning algorithms to assess the optimal application of information from the relationship and pattern analyses. Resulting velocity models will be used to generate final PSET volumes in order to determine if there are meaningful refinements to the PSET volumes compared to those generated from simple, layer cake models like those discussed herein.

5. PRELIMINARY RESULTS

Using the PSET volumes derived using simple, layer cake velocity models and preliminary resistivity volumes inverted from MT data, we have begun to assess their efficacy for targeting geothermal permeability in the subsurface. At San Emidio the known geothermal reservoir lets us rigorously compare the data volumes to geothermal permeability. At Crescent Valley the subsurface is much less constrained; however, the range-front fault system and hot springs provide information about where reservoir fluids discharge to surface and possible paths between the surface and a geothermal reservoir at depth. Drilling, geology, and geophysics contribute to the structural models that we use to evaluate PSET and resistivity volumes, especially interpretation of faults and stratigraphy from 2-D gravity modeling.

5.1 San Emidio PSET and Resistivity

Figure 9 shows discrete microseismic events and PSET acoustic energy as summed Z-scores for each XY location, creating a 2-D representation of PSET results. The northeastern most corner of the data volume shows elevated energy (warm colors) spatially associated with the southernmost production well 61-21. Fracture permeability associated with the geothermal reservoir continues north from this well and also is intersected by well OW-9 and the northern production wells, 75-16, 75B-16, and 76-16. A swath of low energy along the east side of the PSET volume and separating well 61-21 from wells to the southwest coincides with a poorly understood barrier, i.e., a low permeability connection, between the currently producing northern reservoir and the newly discovered southern reservoir based on multi-day flow testing of the southern wells. The eastern margin of the southern reservoir, as currently understood and defined by high permeability, is marked by wells 45-21 and 28-21 which are hot (>160C) but tight with poor connections to the reservoir.
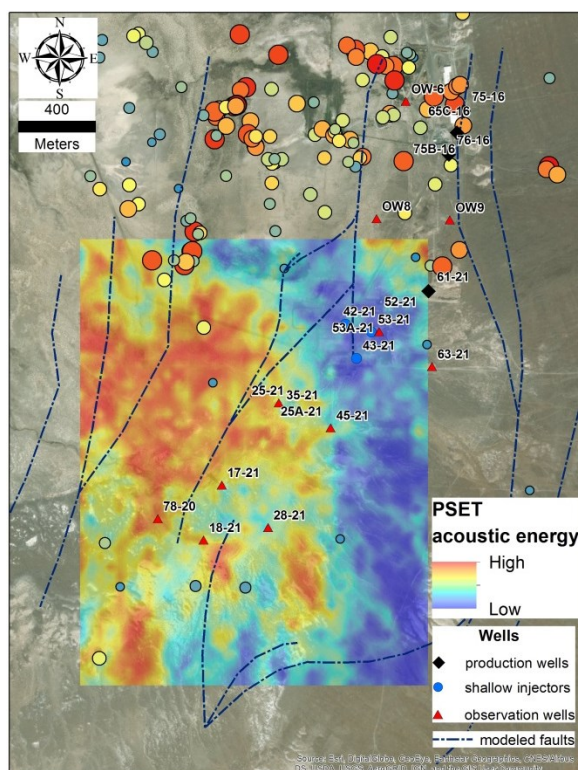
Figure 9: San Emidio PSET volume, discrete microseismic events, and modeled faults. PSET volume Z-scores are summed at each XY locations to give a 2-D representation of the dataset. Discrete events are cool to warm and small to large with increasing energy. PSET volume was processed after filtering out the energy associated with the bulk of discrete events.

Discrete microseismic events (Figures 9 and 10) occurred primarily during power plant shut down (all production pumps and injection stopped) and during the early part of the subsequent plant startup. Similar associations of increased microseismic activity during plant shutdowns have been observed at the Brady Hot Springs geothermal field, Churchill County, NV (Cardiff et al., 2018) and the Blue Mountain geothermal field, Humboldt County, NV (Cladouhos, pers. comm). The majority of the events occurred in hot, tight rocks

west of the northern reservoir, and in three dimensions they form a body that dips gently to the west. Focal mechanisms derived from a few of the largest events show a range of orientations and displacements including examples of strike-slip, low-angle slip, and non-double-couple solutions. The latter may be important as they have been associated with geothermal systems, fluid flow events, and volcanic tremor (Julian, 1994; Julian et al. 1998). Our current working hypothesis, similar to that proposed by Cardiff et L (2018), is that the local stress state is equilibrated with conditions of power plant operation (>95% capacity factor), whereas during shutdown, the rock mass undergoes strain to accommodate changes in pressure and fluid flow. These effects may be more prevalent in tight rocks adjacent to the permeable reservoir, rather than highly permeable parts of the reservoir with relatively large aperture fractures. The controls on these events in time and space are still under investigation.
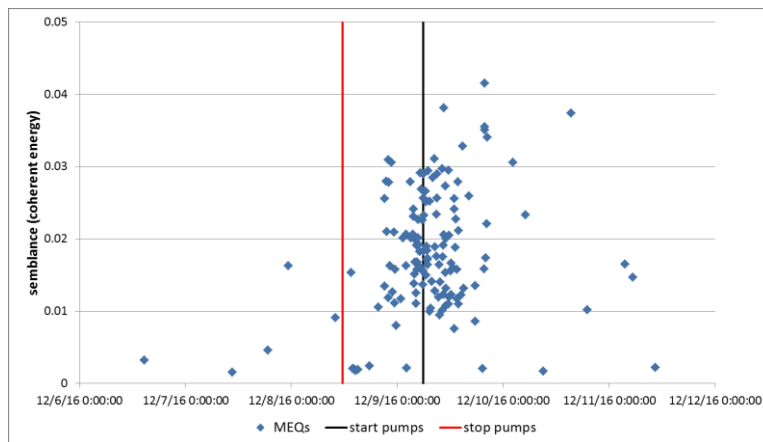
Figure 10: Discrete microseismic events versus time at San Emidio. Events mainly occur during plant shut down and subsequent startup.

In three dimensions PSET energy can be compared to modeled faults and well reservoir intersections. Figure 11 shows PSET energy mapped onto dominantly north-striking and west-dipping faults, locally connected by steeply dipping, northeast-striking linkage structures, and onto "mechanical" basement. Simple 2-D gravity modeling using lower density "basin fill" and higher density "basement" effectively demarcates the transition from weak, clay altered volcaniclastic rocks into the underlying, stronger, silicified lava and tuff that host the geothermal reservoir making it a close proxy for top of the reservoir. Similar to the 2-D representation of Figure 9, high energy characterizes the basement surface west of the low energy eastern boundary of the reservoir. The high energy also occurs along segments of faults through the drilled reservoir and on subparallel faults to the west. The high energy areas shown in Figure 11 closely match the current understanding of the southern reservoir based on limited drilling.
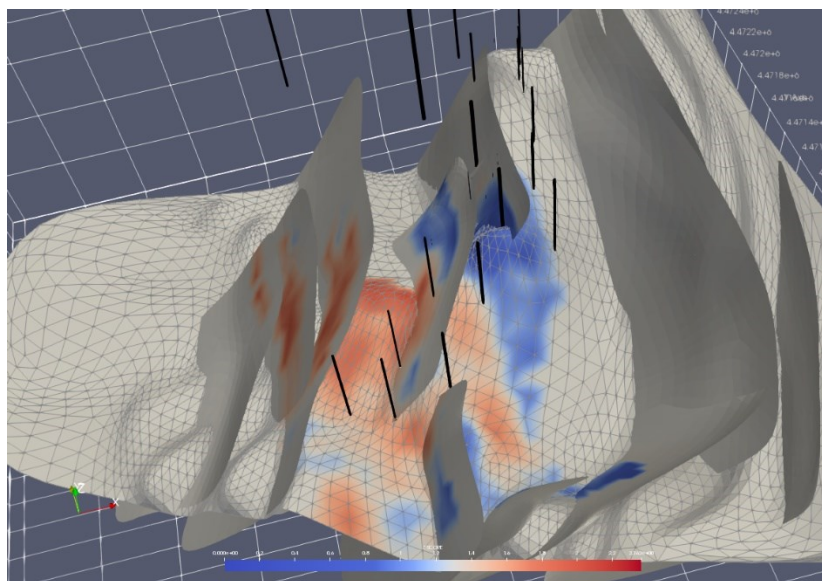
Figure 11: Oblique view looking down and to the north of San Emidio PSET volume mapped onto faults and "mechanical" basement (gray-edged triangulation), a close proxy to the top of the geothermal reservoir. Colors from cool to warm represent increasing acoustic energy (represented by Z-scores). Wells are shown as black cylinders.

The resistivity profiles at San Emidio show large scale structure associated with the main range-front fault that is similar to velocity modeled along co-spatial seismic lines. The survey area is covered with low resistivity sediments (1-10 Ohm-m) that overlie more resistive volcanic and metamorphic rocks at depth (100-1000 Ohm-m). The range-front fault that bounds the western side of the

northern Lake Range is clearly identified by the contrast between the high resistivity footwall and the low resistivity hanging wall, and work is ongoing to investigate finer scale structure. When the preliminary resistivity volume is mapped onto faults and mechanical basement (Figure 12), anomalously low resistivity (conductive geothermal reservoir) maps onto a subtle, faulted ridge into which most drilling has been completed. Though all wells do not intersect highly permeable reservoir, they are all hot and intersect mechanically strong, silicified lava, tuff and metamorphic rock at depth, i.e., reservoir rocks. The resistivity thus far provides a somewhat coarse scale view of structure and potentially maps not only the high permeability reservoir, but also adjacent, lower permeability rocks that provide reservoir storage and are saturated with geothermal brine.
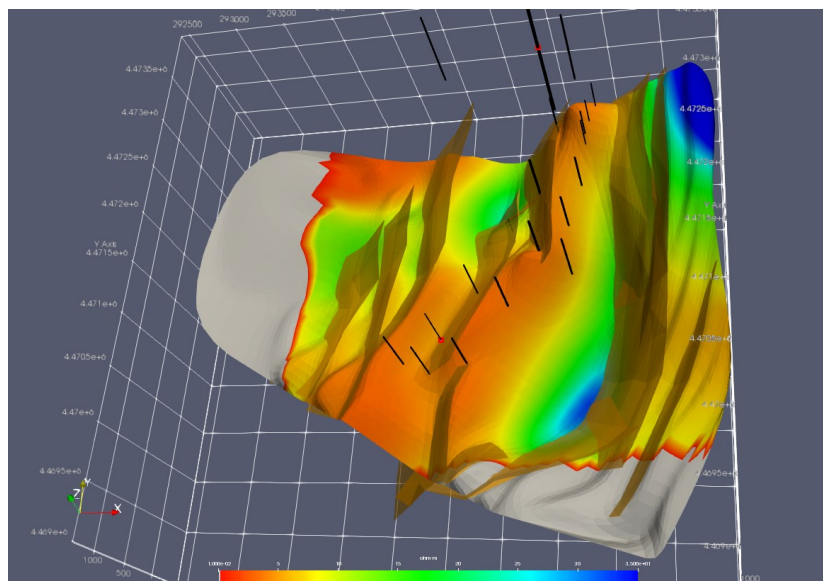
Figure 12: Oblique view looking down and to the north of San Emidio resistivity volume mapped onto faults and "mechanical" basement, a close proxy to the top of the geothermal reservoir. Warm to cool colors map low to high resistivity. Wells are shown as black cylinders.

5.2 Crescent Valley PSET and Resistivity

At Crescent Valley there is much less known about the subsurface and preliminary results are mainly limited to visualizations of new datasets. Figure 13 shows PSET energy summed at each XY location to give a 2-D representation. An anomalous area of high energy occurs down dip and basinward from the hot springs and is elongated in directions subparallel to mapped and interpreted faults associated with the range-front step-over. Using a similar strategy as at San Emdio, data volumes also have been mapped onto faults measured at surface and interpreted from seismic profiles and modeled gravity. Figure 14 shows PSET energy mapped onto faults; anomalous segments of the faults are generally located down dip and basinward from the hot springs at the southwest end of the range-front step-over. Similar to San Emidio, low resistivity sedimentary rocks overlie more resistive granodiorite +/- Tertiary volcanic rocks +/- Paleozoic sedimentary rocks. The resistivity structure recovered from MT inversion shows the main range-front fault, as well as two other range-front-parallel faults, and variable basin fill thickness overlying the basement. A slice through the resistivity volume that runs through the hot springs and is oriented perpendicular to the range-front fault shows conductive geothermal upflow associated with the range front and outflow into the basin, consistent with heat flow anomalies defined by 1970s temperature gradient drilling.
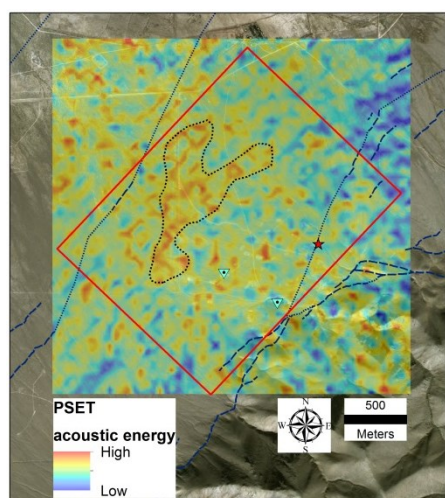
Figure 13: Crescent Valley PSET volume Z-scores are summed at each XY locations to give a 2-D representation of the dataset. Dotted black outline encompasses the anomaly described in the text. Red star is well 67-3. Cyan triangles are hot springs. Dark blue faults are from McConville et al. (2017) but do not include all that are modeled in the subsurface.
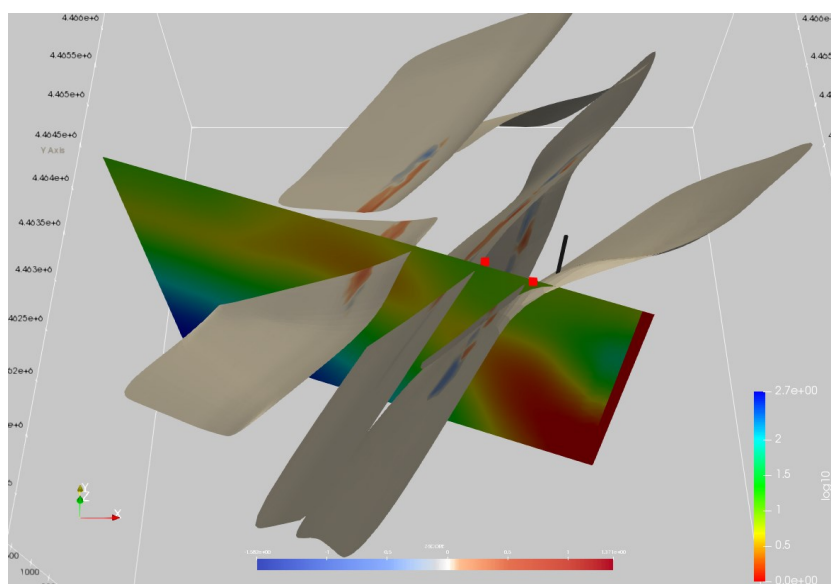
Figure 14: Oblique view looking down and to the north of Crescent Valley PSET volume mapped onto faults with cool to warm colors representing low to high energy. A slice through the resistivity volume shows low to high resistivity represented by hot to cold colors.

6. CONCLUSIONS

Preliminary analyses of new passive seismic and magnetotelluric data collections at San Emidio and Crescent Valley suggest that they will be useful for creating robust 3-D permeability maps. At both locations, resistivity contrasts map large-scale structure associated with range-front faults, and patterns of low resistivity correspond to areas saturated with geothermal brine. At San Emidio areas of high energy mapped with PSET correlate with areas of known permeability, and areas of low energy mark the currently understood boundaries of the newly discovered southern reservoir. The correlation between high energy and permeability is further strengthened with PSET data mapped onto faults and the top of reservoir rocks. Discrete microseismic events generally were not closely associated with high permeability parts of the reservoir(s); instead, they primarily occurred in adjacent rocks following plant shut down and during the beginning of the subsequent restart. At Crescent Valley the main range-front fault and subparallel faults in the hanging wall show high energy down dip and basinward from hot springs.

As the project continues, we will be developing a cooperative seismic-MT inversion methodology to not only enhance their utility for mapping geothermal permeability, but also to generate more robust velocity models than the simple layer cake models thus far used for PSET processing. Updated and refined velocity models will be used to process final PSET volumes. At the same time, additional effort will be directed toward identifying microseismic events and resolving focal mechanisms so that stress and geomechanics potentially can be included in the permeability map generation. Once final 3-D permeability maps are complete, we will propose drill targets to test

them. If successful, a complete methodology will be presented to detail how a robust 3-D geothermal permeability map can be created to more accurately target geothermal reservoirs.

REFERENCES

Bennett, R.A., Wernicke, B.P., Niemi, N.A., Friedrich, A.M., and Davis, J.L., 2003, Contemporary strain rates in the northern Basin and Range province from GPS data, Tectonics, v. 22, No. 2, p. 1-31.

Bonham, H.F., and Papke, K.G., 1969, Geology and mineral deposits of Washoe and Storey Counties, Nevada, Nevada Bureau of Mines and Geology Bulletin 70, scale 1:250,000, 140 p.

Cardiff, M., Lim, D.D., Patterson, J.R., Akerley, J., Spielman, P., Lopeman, J., Walsh, P., Singh, A., Foxall, W., Wang, H.F., Lord, N.E., Thurber, C.H., Fratta, D., Mellors, R.J., Davatzes, N.C., and Feigl, K.L., 2018, Geothermal production and reduced seismicity: Correlation and proposed mechanism, Earth and Planetary Science Letters, 482, p. 470-477.

Casteel, J., Pullammanapallil, S., and Mellors, R., 2016, Estimating Subsurface Permeability with 3D Seismic Attributes: A Neural Net Approach, PROCEEDINGS, Forty-first Workshop on Geothermal Reservoir Engineering, Stanford University, Stanford, California, February 22-24, 2016, 8 p.

Drakos, P.S., 2007, Tertiary stratigraphy and structure of the southern Lake Range, northwest Nevada: Assessment of kinematic links between strike-slip and normal faults in the northern Walker Lane [M.S. Thesis], University of Nevada, Reno, 165 p.

Duncan, P.M. and Eisner, L., 2010, Reservoir characterization using surface microseismic monitoring, Geophysics, vol. 75, no. 5, p. 75A139-75A146.

Egbert, G.D., 1997. Robust multiple station magnetotelluric data processing. Geophysical Journal International 130, 475–496.

Eneva, M., Falorni, G., Teplow, W., Morgan, J., Rhodes, G., and Adams, D., 2011, Surface deformation at the San Emidio Geothermal Field, Nevada, from satellite radar interferometry, Geothermal Resources Council Transactions, vol. 35, p. 1647-1654.

Faulds, J.E., Coolbaugh, M.F., Hinz, N.H., Cashman, P.H., and Kratt, C., Dering, G., Edwards, J., Mayhew, B., and McLachlan, H., 2011, Assessment of favorable structural settings of geothermal systems in the Great Basin, western USA: Geothermal Resources Council Transactions, v. 35, p. 777-784.

Faulds, J.E., Hinz, N.H., Coolbaugh, M.F., dePolo, C.M., Siler, D.L., Shevenell, L.A., Hammond, W.C., Kreemer, C., and Queen, J.H., 2016, Discovering Geothermal Systems in the Great Basin Region: An Integrated Geologic, Geochemical, and Geophysical Approach for Establishing Geothermal Play Fairways, PROCEEDINGS, Forty-first Workshop on Geothermal Reservoir Engineering, Stanford University, Stanford, California, February 22-24, 2016, 15 p.

Geiser, P., Lacazette, A., and Vermilye, J., 2012. Beyond "dots in a box." First Break, Vol. 30, p. 63-69.

Hammond, W.C. and Thatcher, W., 2005, Northwest Basin and Range tectonic deformation observed with the Global Positioning System, 1999-2003, Journal of Geophysical Research, v.110, 12 p.

Hammond, W.C., Kreemer, C., and Blewitt, G., 2009, Geodetic constraints on contemporary deformation in the northern Walker Lane: 3. Central Nevada seismic belt postseismic relaxation, in Oldow, J.S., and Cashman, P.H., eds., Late Cenozoic Structure and Evolution of the Great Basin-Sierra Nevada Transition:Geological Society of America Special Paper 447, p. 33-54.

Jeremic, A., Thornton, M., and Duncan, P., 2016, Ambient passive seismic imaging with noise analysis, SEG Technical Program Expanded Abstracts 2016, p. 2586-2590.

Julian, B. R., 1994, Volcanic tremor: Nonlinear excitation by fluid flow, J. Geophys. Res., 99, p. 11859-11877.

Julian, B.R., Miller, A.D., and Foulger, G.R., 1998, Non-Double-Couple Earthquakes, 1., Reviews of Geophysics, 36, 4, p. 525-549.

Lacazette, A. and Morris, A., 2015, A New Method of Neostress Determination from Passive Seismic Data: Unconventional Resources Technology Conference, San Antonio, Texas, USA, 20-22 July 2015, 12pp.

McConville, E.G., Faulds, J.E., Hinz, N.H., Ramelli, A.R., Coolbaugh, M.F., Shevenell, L., Siler, D.L., and Bourdeau-Hernikl, J., 2017, A Play Fairway approach to geothermal exploration in Crescent Valley, Nevada, Geothermal Resources Council Transactions, vol. 41, p. 1213-1221.

Rhodes, G.T., Faulds, J.E., and Teplow, W., 2010, Structural controls of the San Emidio Desert Geothermal Field, northwestern Nevada, Geothermal Resources Council Transactions, vol. 34, p. 819-822.

Rhodes, G.T., Faulds, J.E., and Ramelli, A.R., 2011, Preliminary Geologic Map of the Northern Lake Range, San Emidio Geothermal Area, Washoe County, Nevada, Nevada Bureau of Mines and Geology Open-File 11-11, 1:24,000 scale, 5p.

Sicking, C., Vermilye, J., Geiser, P., Lacazette, and A., Thompson, L., 2012, Permeability field imaging from microseismic, Society of Exploration Geophysics Annual Meeting, 4-9 November, Las Vegas, Nevada 1383, 5 p.

Teplow, W. and Warren, I., 2015, Finding Large Aperture Fractures in Geothermal Resource Areas Using a Three-Component Long-Offset Surface Seismic Survey, PSInSAR and Kinematic Structural Analysis, https://www.osti.gov/scitech/biblio/1213113-finding-large-aperture-fractures-geothermal-resource-areas-using-three-component-long-offset-surface-seismic-survey-psinsar-kinematic-structural-analysis, 52p.

Vozoff, K., 1991. The magnetotelluric method. In: Nabighian, M.N. (Ed.), Electromagnetic Methods in Applied Geophysics, vol. 2B. Soc. Explor. Geophys., Tulsa, OK, USA, pp. 641–711.

Wood, J.D., 1990, Geology of the Wind Mountain gold deposit Washoe County, Nevada, *in* Raines, G.L., Lisle, R.E., Schafer, R.W., and Wilkinson, W.H., eds., Geology and ore deposits of the Great Basin: Symposium proceedings: Geological Society of Nevada, p. 1051-1061.